JOURNAL OF CATALYSIS 30, 260–275 (1973)

Adsorption and Decomposition of Formaldehyde on Tungsten (100) and (111) Crystal Planes

JOHN T. YATES, JR., THEODORE E. MADEY, AND MILES J. DRESSER*

National Bureau of Standards, Washington, D. C. 20234

Received February 27, 1973

The chemisorption of formaldehyde at ~100 K has been investigated on two single crystal planes of tungsten, W(100) and W(111). At low H_2CO coverages, only H_2 and CO are observed as thermal desorption products. At higher H_2CO coverages both CH_4 and CO_2 are observed as additional desorption products. Work function and flash desorption measurements indicate that the dissociative adsorption of H_2CO into H(ads) and CO(ads) is accompanied at higher surface coverages by the formation of other surface complexes.

A detailed comparison of W(100) with W(111) indicates that crystallographic differences play a minor role in the surface catalyzed decomposition of H_2CO by tungsten.

I. Introduction

The temperature-programmed thermal desorption method (commonly termed flash desorption) has been extensively applied to the investigation of diatomic molecule adsorption by both polycrystalline (*1–3*) and single crystal transition metal surfaces (*4–6*). There are, however, fewer examples of the application of this method (*7–9*) to the study of more complex molecules which yield either fragment desorption products or catalytically produced species containing entirely different internal chemical bonds.

In this paper we have employed the flash desorption technique to examine the role of substrate crystallography on the chemisorption and surface-catalyzed decomposition of formaldehyde by tungsten. Two crystal planes of bcc tungsten were examined: The atomically rough W(111) plane, and the smoother cube face plane, W(100). We have also used field emission microscopy and work function measurements to follow H_2CO decomposition on tungsten.

Previous flash desorption studies have been made of pure H_2 chemisorption on W(100) (*4, 5*) and W(111) (*10, 11*), of pure CO on W(100) (*12–15*) and of the interaction between H_2 and CO adsorbed on W(100) (*12*). In addition, the adsorption behavior of CH_4 on both W(100) (*16*) and W(111) (*11*) and CO_2 on W(100) (*15*) have been investigated (CH_4 and CO_2 are decomposition products of adsorbed H_2CO). These previous investigations form a sound experimental basis for comparison with H_2CO decomposition on W(100) and W(111).

We note the *lack of attention* given to the chemisorption of formaldehyde. For example, there are no papers concerned with adsorption and catalytic formaldehyde decomposition in Vol. 1–23 of *J. Catal.* (1962–1971). An early paper deals with the thermal decomposition of H_2CO over Pt catalysts (*17*). There is also a recent observation of H_2CO adsorption behavior on Pt (111) (*18*), where only H_2 and CO thermal desorption products were observed. It is of interest to note that

* Visiting Scientist, on leave from Department of Physics, Washington State University, Pullman, WA.

heterogeneous reactions involving HCO (ads) on glass are proposed in experiments involving H_2CO photolysis (*19*).

As will be discussed, the interaction of H_2CO with tungsten single crystals is complex. At low initial H_2CO coverages ($\lesssim 0.5$ monolayers), the only gaseous desorption products observed during flash desorption are H_2 and CO. At higher H_2CO coverages, both CH_4 and CO_2 are observed as additional gaseous desorption products. While the details of the H_2CO decomposition processes are different on W(100) and W(111), the gross features (decomposition products, distribution of products' binding states, and work function behavior) are remarkably similar.

II. Experimental Methods

The Pyrex ultrahigh vacuum (uhv) apparatus (base pressures $\sim 1 \times 10^{-10}$ Torr) and crystal preparation have been described previously (*5*, *16*). This apparatus permits the use of a focused beam of light, external to the vacuum vessel, to raise the temperature of a thin single crystal disc at a nearly linear rate for programmed flash desorption. The sample crystals were nearly circular discs ($\sim$6 mm in diameter and $\sim$0.12 mm thick), ground and polished with the appropriate crystallographic orientation on both sides and supported by a thin tungsten wire. The exposed surface areas were $\sim$95% of the designated orientation, with $\sim$5% edge effects. The temperature of each crystal was measured using a W/W–26% Re thermocouple (0.025 mm diameter wires) welded to its edge. The crystals were cleaned prior to each adsorption sequence by heating in good vacuum to 2500 K via electron bombardment from a pure tungsten filament. Frequent heat treatment of the crystals in O_2(g) was done to remove possible impurity carbon from the surface. A quadrupole mass spectrometer operating at 35 eV electron energy and 0.25 mA emission current was used to measure the partial pressures of the various gases during adsorption and flash desorption; it was frequently calibrated against a Bayard-Alpert ionization gauge. Gauge sensitivity ratios were taken from P. A. Redhead and J. P. Hobson and E. V. Kornelson, "The Physical Basis of Ultrahigh Vacuum" Chapman and Hall, London, 1968, Table 7.2: $[H_2/N_2] = 0.4$; $[CH_4/N_2] = 1.37$; $[CO/N_2] = 1.1$. The gauge was normally turned off during adsorption experiments.

Much of the data in this paper is displayed as plots of gas phase partial pressure Δp, observed during heating of the crystal by the focused light (typical heating rates were $\sim$20 K s^{-1}). These plots of Δp vs temperature (or time) are termed desorption spectra. The integrated area under a desorption spectrum is proportional to the coverage θ of that species observed to desorb and is usually expressed in fractions of a monolayer. One monolayer, is defined here as the saturation coverage of the *pure* species in question on the clean tungsten substrate at $\sim$100 K.

Most of the flash desorption experiments were performed using liquid nitrogen cooling of the crystal and its support assembly. The cooled surfaces rapidly pumped such species as CO, CH_4, and CO_2 with varying rates, so that an absolute coverage measurement is virtually impossible. Hence, desorption yields of all species are expressed either as fractions of monolayers or as

$$\int_{\Delta t} i_\chi^+ dt$$

where i_χ^+ is the quadrupole mass spectrometer ion current due to species χ which desorbs completely during the time interval Δt as the crystal temperature is raised.

An electron gun, directed at the rear of the crystal, was used to measure work function changes during adsorption, using an electron retardation method (*5*, *16*). This measurement of work function does not disturb the adsorbed layer due to electron impact effects because the incident electrons have low kinetic energies when they reach the crystal surface.

Formaldehyde gas was prepared in an external vacuum system by heating paraformaldehyde crystals to 350 K and distilling H_2CO(g) into a reservoir at 77 K where multiple freeze–thaw–vaporize puri-

fication cycles were carried out. H_2CO was then vaporized at 195 K and transferred directly into a previously baked 1000 cm^3 Pyrex bulb where it was stored at a pressure of ~0.1 Torr. H_2CO(g) could be admitted directly from this storage bulb into the uhv system by means of a stainless steel leak valve. Depending upon unknown experimental differences in the nature of different baked storage bulbs, formaldehyde vapor at ~0.1 Torr could be stored at 300 K for periods ranging from days to weeks without appreciable decomposition or catalytic conversion to other products. In Fig. 1A is shown the mass spectrum of freshly prepared H_2CO, containing a small amount of CO_2 and H_2 impurity. Following 6 days storage, new mass peaks at m/e = 60, 32, 31, 15, and 13 are observed (Fig. 1B). There are a number of possible impurities which could produce mass 60, namely, trioxane $(CH_2O)_3$, acetic acid, methyl formate ($HCOOCH_3$) and glycol aldehyde (CH_2OHCHO). On the basis of the absence of peaks at m/e = 89 and 61, we can eliminate trioxane as an impurity. Acetic acid should exhibit peaks at m/e = 45, 43, and 42, and can therefore be eliminated also. We do not know the mass spectrum of glycolaldehyde. However, the observed extra-peak ratios are consistent with the impurity being methyl formate [experimental ratios shown along with API (*20*) ratios in parentheses]: 60:31 = 0.28 (0.28); 32:31 = 0.34 (0.34); 45:31 = 0.018 (0.0144); 18:31 = 0.055 (0.0234). Furthermore, Walker (*21*) reports that methyl formate is a common impurity in formaldehyde produced from paraformaldehyde. There is, however, little formic acid present since m/e peaks at 45 and 46 are absent.

Because of the buildup of methyl formate impurity, the mass spectrum of H_2CO was monitored prior to experiments, and fresh H_2CO was generated frequently during the course of this work.

III. Results

A. *Coadsorption of H_2 + CO on W(100) at ~110 K*

Before discussing H_2CO decomposition on tungsten, it is appropriate to recall the essential features of the coadsorption of H_2 and CO on W(100); the details of this interaction have been published previously (*12*). The effect of CO addition to an H_2 monolayer on W(100) at ~110 K is illustrated in the desorption spectra of Fig. 2. Figure 2a is the desorption spectrum for hydrogen corresponding to the saturation coverage of H_2 on W(100) at ~110 K; the familiar β_2 and β_1 binding states are clearly seen. When the pure H_2 monolayer formed by adsorption at ~110 K is then exposed to 66 × 10^{-6} Torr s of gaseous CO, the hydrogen desorbs with a new distribution of binding states (the ν states) seen in Fig.

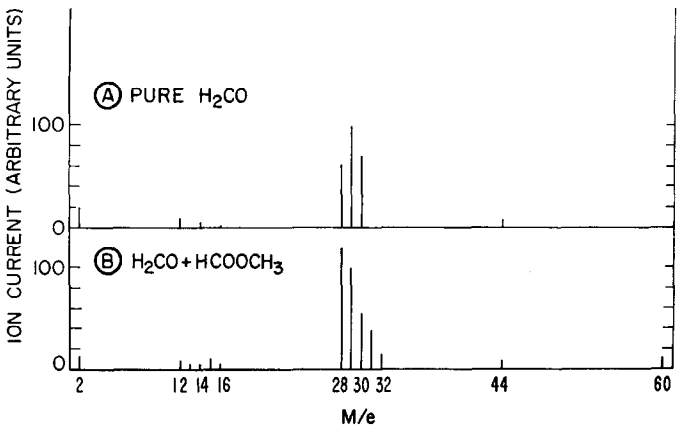

FIG. 1. Comparison of mass spectrum of pure formaldehyde with the mass spectrum of methyl formate-contaminated formaldehyde. Electron energy V_e = 70 eV, total gas pressure = 2 × 10^{-8} Torr.

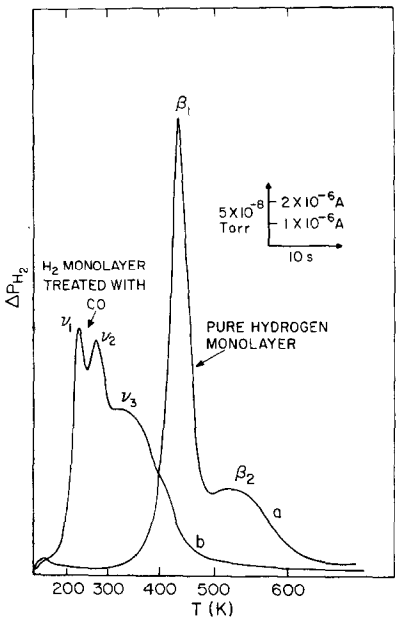

FIG. 2. Desorption spectra for saturation coverage of hydrogen adsorbed on W(100) at $T_0 \simeq 110$ K. (a) Desorption from a pure hydrogen layer; (b) desorption of hydrogen following exposure of the hydrogen layer to 66×10^{-6} Torr s of CO. [A = amperes ion current from mass spectrometer; s = seconds.]

2b. The coadsorption of CO with hydrogen on W(100) results in a weakening of the hydrogen–metal bonds and the conversion of hydrogen to new, lower energy binding states. The fractional coverage of hydrogen in the ν states is a function of CO coverage; in the limit of complete conversion (cf. Fig. 2b), when the CO coverage has become ~0.6 monolayer, the hydrogen coverage is diminished to ~0.9 monolayer.

B. H_2CO on W(100) at ~110 K: Flash Desorption

The adsorption and decomposition of H_2CO on W(100) was studied as follows. The crystal was flashed clean *in vacuo* and cooled to ~110 K; H_2CO(g) was admitted to the vessel for a fixed exposure (expressed as Torr s). After pumping away the H_2CO (g), the crystal was heated using the focused light, and the flash desorption spectra of the various desorption products were recorded.

Figure 3 shows a series of flash desorption spectra for H_2 desorption following increasing exposures of the W(100) crystal to H_2CO(g); the crystal was cleaned by flashing to 2500 K prior to each data curve. Spectra a to f of Fig. 3, in which the H_2 coverage θ is $\leq$0.5 monolayer, are similar to H_2 desorption spectra seen during studies of coadsorption of H_2 and CO (*12*): the common features are the shift of the maxima to lower temperatures as coverage

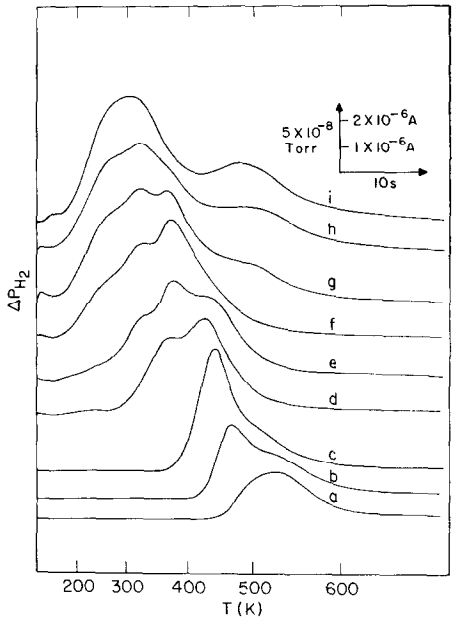

FIG. 3. Desorption spectra for desorption of H_2 from H_2CO layers adsorbed on W(100) at $T_0 \simeq$ 110 K. Mass 2 ion current is plotted vs crystal temperature.

curve	H_2 coverage, θ (relative to "pure" H_2 monolayer)	H_2CO exposure[a] ($\times10^{-6}$ Torr s)
a	0.16	0.7
b	0.21	1.5
c	0.29	1.7
d	0.34	1.9
e	0.41	3.0
f	0.50	3.8
g	0.59	5.0
h	0.50	5.6
i	0.69	7.9

[a] 1×10^{-6} Torr s = 3.7×10^{14} H_2CO molecules/cm^2 incident flux.

increases and the multiplicity of peaks in the temperature region 200–400 K. Compare the ν states of Fig. 2b with curves e and f of Fig. 3; three major peaks in the same temperature region (200–400 K) are seen in both cases, although the relative amplitudes of the 3 peaks are different. Such differences may be due to the different CO:H ratios achieved in the H_2 + CO experiments, compared to the H_2CO adsorption experiment. Curves g to i of Fig. 3 ($\theta_{H_2} \gtrsim 0.5$ monolayer) exhibit a new feature not seen at lower coverages: a new peak appears in the desorption spectra with its maximum at ~500 K. In addition, the detail in the region 200–400 K is obliterated, and we observe a single, broad peak.

Figure 4 shows a series of flash desorption spectra corresponding to liberation of CH_4 from H_2CO adsorbed on W(100) at ~110 K. Significant CH_4 desorption (Fig. 4d) is observed at roughly the same H_2CO exposure as is necessary to produce the 500 K peak in the H_2 desorption spectra (Fig. 3g), that is, at H_2CO exposures $\gtrsim 4 \times 10^{-6}$ Torr s. The intensities of the methane peaks grow as the H_2CO exposure is increased. For comparison, the broken curve in Fig. 4 is a methane desorption spectrum observed for a pure CH_4 layer which is physically adsorbed on W(100) (*16*). The differences between the broken and solid curves of Fig. 4 indicate that the CH_4 produced following adsorption of H_2CO arises from surface-catalyzed decomposition of the H_2CO as the surface is heated during desorption. At least the major portion of the CH_4 is *not* present as an adsorbed entity on the surface at the adsorption temperature, but is produced thermally during the heating process.

In Figure 5, a series of flash desorption spectra illustrate the kinetics of desorption of another product from adsorbed H_2CO layers: gaseous CO_2. As in the case of methane, the CO_2 is only observed following H_2CO exposures $> 4 \times 10^{-6}$ Torr s. The threshold H_2CO exposure for CO_2 desorption appears slightly higher than that for CH_4 desorption.

Another thermal desorption product from the adsorbed H_2CO was CO. However,

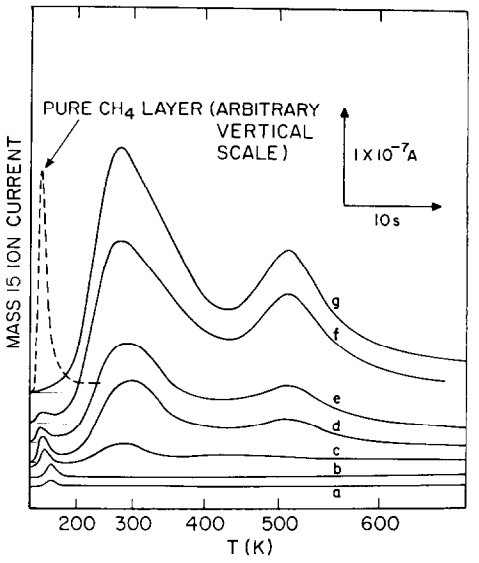

FIG. 4. Desorption spectra for CH_4 desorbed from H_2CO layers adsorbed on W(100) at $T_0 \simeq 110$ K. Mass 15 (CH_3^+) ion current is plotted vs crystal temperature (K).

Curve	H_2CO_6 exposure ($\times 10^{-6}$ Torr s)
a	1.0
b	1.9
c	3.0
d	4.3
e	5.0
f	6.5
g	6.6

The broken curve is a desorption spectrum for CH_4 desorbed from a pure CH_4 layer adsorbed on W(100) [cf. Ref. (*16*)].

since most of the CO desorbed at tungsten temperatures greater than those achievable using the focused light source (i.e., $\gtrsim 900$ K), we did not perform a systematic study of the CO flash desorption behavior. Flash desorption studies of pure CO from W(100) have been reported previously (*12–15*).

The above results are consistent with the following picture for H_2CO adsorption on W(100). At low coverages ($\theta \lesssim 0.5$), and upon heating, the adsorbed layer behaves in similar fashion to mixtures of H(ads) and CO(ads), and only H_2 and CO are liberated. At higher coverages, new inter-

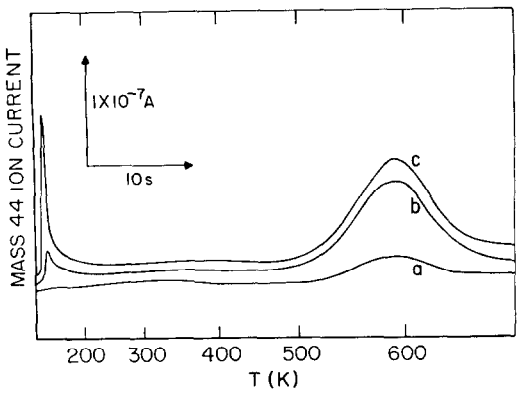

FIG. 5. Desorption spectra for CO_2 desorbed from H_2CO layers adsorbed on W(100) at $T_0 \simeq 110$ K. Mass 44 ion current is plotted vs crystal temperature (K).

Curve	H_2CO exposure ($\times 10^{-6}$ Torr s)
a	5.3
b	6.7
c	10.2

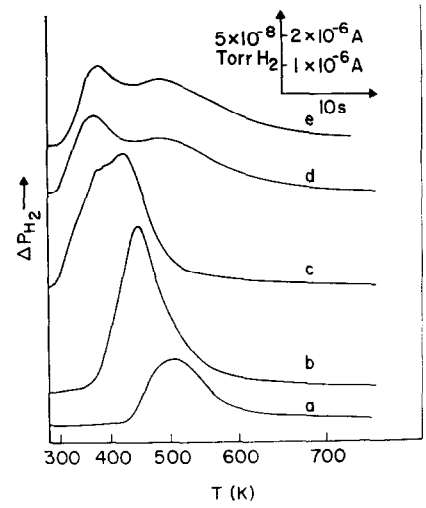

FIG. 6. Desorption spectra for H_2 desorbed from H_2CO layers adsorbed on W(100) at $T_0 \simeq 273$ K. Mass 2 ion current is plotted vs crystal temperature (K).

Curve	H_2CO exposure ($\times 10^{-6}$ Torr s)
a	0.5
b	1.5
c	3.5
d	4.6
e	34

mediate species are formed; during heating these species thermally decompose to yield CH_4 and CO_2 as additional desorption products.

It is of interest to compare Fig. 3i (H_2 desorption) with Fig. 4g (CH_4 desorption). The two major peaks in both spectra have roughly the same relative amplitudes and occur in roughly the same temperature regimes, suggesting the same rate controlling steps involving the decomposition of adsorbed surface complexes lead to H_2 and CH_4 products.

C. H_2CO on W(100) at 273 K: Flash Desorption

In order to assess the effect of adsorption temperature on the decomposition of adsorbed H_2CO, a series of experiments were carried out with the W(100) crystal at 273 K during adsorption of H_2CO. Figure 6 shows a sequence of H_2 flash desorption spectra obtained after various exposures of W(100) to H_2CO. These data are similar to those obtained following adsorption at ~110 K (Fig. 2). In Fig. 6, as the H_2CO exposure increases from 0.5 to 3.5×10^{-6} Torr s, the H_2 desorption maximum shifts to lower temperatures and structure appears below $T \sim 400$ K. At exposures $\gtrsim 4.6 \times 10^{-6}$ Torr s, the new broad peak at ~500 K appears. It thus appears that the adsorption processes at both 110 and 273 K are similar, and that only the low temperature desorption states ($T \lesssim 273$ K) seen in Fig. 2 are missing in Fig. 6.

The fact that major amounts of hydrogen remain on the W(100) surface in the limit of heavy H_2CO dosage contrasts markedly with CO adsorption experiments involving CO exposure to a hydrogen monolayer at 273 K (*12*). The coadsorption measurements show that hydrogen can be completely displaced by CO. This difference in behavior is indicative once again that at high H_2CO exposures, surface intermediates other than H(ads) and CO(ads) are produced on W(100) even at 273 K,

and these intermediates are responsible for hydrogen retention in the adsorbed layer.

As shown in Fig. 7a and b, the methane desorption spectra seen following adsorption of H_2CO at 273 K are also similar to those obtained following adsorption at ~110 K (Fig. 3). As in the case of H_2 desorption, only the low temperature part of the CH_4 desorption spectra are missing upon adsorption at 273 K. Curves a and b of Fig. 7 also demonstrate the similarity between the mass 15 (CH_3^+) and mass 16 (CH_4^+) desorption traces: this comparison conclusively demonstrates that we are measuring CH_4 by monitoring mass 15 in the desorption experiments. Curve c of Fig. 7 indicates that a small quantity of hydrocarbon having mass 29 as a cracking fraction (probably C_2H_6) also desorbs from the surface following a H_2CO exposure of 7×10^{-6} Torr onto the W(100) crystal at 273 K. As in the case of CH_4 and CO_2, no mass 29 peak was seen for H_2CO exposures $\lesssim 5 \times 10^{-6}$ Torr s.

D. Coadsorption of H_2 + CO on W(111) at 104 K: Flash Desorption

Before examining the details of H_2CO decomposition on W(111), it is appropriate to consider the coadsorption of H_2 and CO on this plane. The effect of CO addition to a hydrogen monolayer formed on W(111) at 104 K is shown in the hydrogen desorption spectra of Fig. 8. In each case, the surface was cleaned at ~2500 K and cooled to 104 K prior to adsorption of the saturation (monolayer) coverage of hydrogen. Exposure of the hydrogen covered surface to various exposures of CO preceded the flash desorption spectra. Figure 8a is the flash desorption spectrum for pure hydrogen; the molecular γ states and the 4 atomic β states reported previously (*10*, *11*) are clearly evident. Following increasing exposure of the H_2 covered surface to gaseous CO, two features are apparent in the hydrogen desorption spectra of curves b, c, and d. Firstly, as CO coverage increases, the binding energy of the adsorbed hydrogen decreases, and new structure appears in the range 200–400 K. Secondly, the hydrogen coverage remaining on the surface decreases upon coadsorption of CO: for

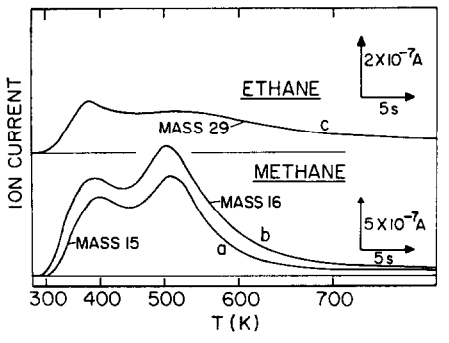

FIG. 7. Desorption spectra for hydrocarbons desorbed from H_2CO layers adsorbed on W(100) at $T_0 \simeq 273$ K. Note differences in ordinate magnitude between curves.

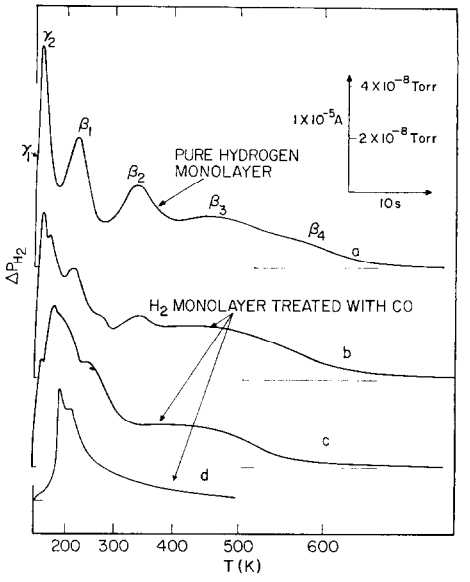

FIG. 8. Desorption spectra for saturation hydrogen layer adsorbed on W(111) following exposure to increasing amounts of CO. $T_0 \simeq 104$ K.

Curve	CO exposure ($\times 10^{-6}$ Torr s)	H_2 coverage relative to saturation coverage on clean W(111)
a	0 (pure hydrogen layer)	1.0
b	0.17	0.95
c	0.62	0.83
d	36	0.27

curve d, only 0.27 monolayer of hydrogen remains after a CO exposure of 36×10^{-6} Torr s. In contrast to the H_2 + CO on W(100) results at ~110 K (*12*), CO rapidly displaces adsorbed hydrogen on W(111) at 104 K. This displacement presumably occurs via a weakening of the hydrogen-metal bonds and a conversion to weakly bound hydrogen species which desorb rapidly at 104 K. For W(100), essentially all of the weakly bound ν states produced upon interaction of CO with adsorbed hydrogen remain "frozen in" on the surface at ~110 K, and loss of hydrogen by desorption at this temperature is slight.

Thus, a comparison of flash desorption results for the W(100) and W(111) planes indicates that there are clear crystallographic and/or electronic effects which produce differences in the interaction of pure H_2 and of CO + hydrogen on W(100) and W(111). As will be seen, the influence of substrate crystallography on formaldehyde decomposition is less pronounced.

E. H_2CO on W(111) at 104 K: Flash Desorption

A series of desorption spectra for the desorption of hydrogen following adsorption of H_2CO on W(111) at various exposures is shown in Fig. 9. These spectra have some features in common with the H_2 desorption data from H_2CO on W(100) shown in Fig. 3. As H_2CO coverage increases, new peaks appear having lower binding energy (i.e., lower desorption peak temperatures). At the highest formaldehyde coverage studied, curve e, two major peaks are apparent at ~350 and ~450 K, which are reminiscent of the two peaks seen at highest H_2CO exposures on W(100).

There are clear differences between the H_2 desorption spectra from H_2 + CO and H_2 desorption from H_2CO layers (Figs. 8 and 9). From the H_2 + CO coadsorption data, it is clear that CO causes appreciable displacement of the adsorbed hydrogen to lower binding energy states which desorb below $T \simeq 300$ K; the total hydrogen coverage *decreases* to as low as 0.27 monolayer via CO displacement. In contrast, increasing exposure of W(111) to H_2CO leads to a monotonic *increase* of hydrogen coverage which is present in binding energy states which desorb at $T > 300$ K (for Fig. 9, curve e, $\theta_{H_2} \simeq 0.8$ monolayer). This is strong evidence that at least at higher coverages, the kinetics of liberation of H_2 from the H_2CO layer are determined by the rate of thermal decomposition of the adsorbed H_2CO molecule or a related intermediate adsorbed species, and that H_2 does not arise from a simple mixture of H(ads) and CO(ads).

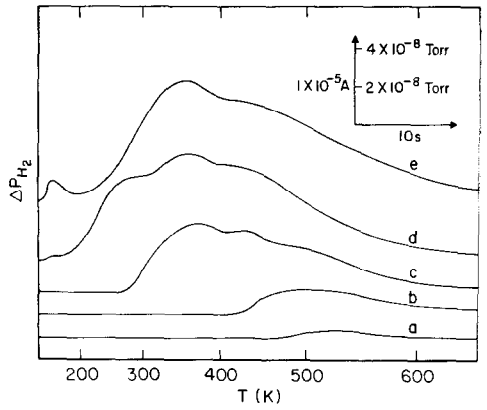

FIG. 9. Desorption spectra for hydrogen desorbed from H_2CO layers adsorbed on W(111) at $T_0 \simeq$ 104 K. Mass 2 ion current is plotted vs crystal temperature.

Curve	Hydrogen coverage, θ (relative to "pure" H_2 monolayer)	H_2CO exposure ($\times 10^{-6}$ Torr s)
a	0.03	0.5
b	0.12	2.4
c	0.41	6.0
d	0.77	17
e	0.81	38

A series of flash desorption spectra for CH_4 desorbed from H_2CO layers adsorbed on W(111) at ~104 K is shown in Fig. 10. Below a H_2CO exposure of $\sim 7 \times 10^{-6}$ Torr s, no CH_4 is liberated upon heating. At higher H_2CO exposures, increasing amounts of CH_4 desorption are seen. Curve d of Fig. 10 shows the presence of two desorption states for CH_4: there is a major peak at ~250 K and a lesser peak at ~500 K.

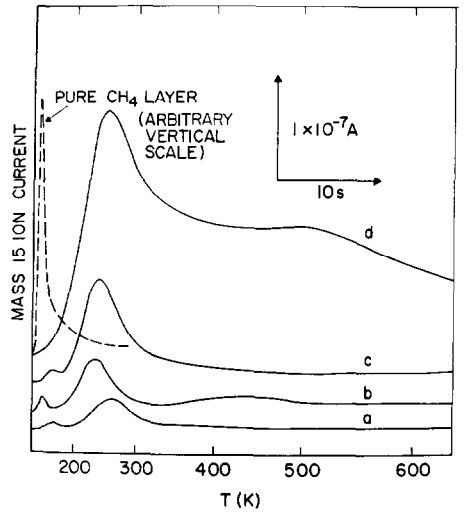

FIG. 10. Desorption spectra for CH_4 desorbed from H_2CO layers adsorbed on W(111) at $T_0 \simeq$ 104 K. Mass 15 (CH_3^+) ion current is plotted vs crystal temperature (K).

Curve	H_2CO exposure ($\times 10^{-6}$ Torr s)
a	8.2
b	8.8
c	13
d	35

The broken curve is a desorption spectrum for CH_4 desorbed from a pure CH_4 layer adsorbed on W(111) [cf. Ref. (*11*)].

These are in the same temperature regions where two more distinct CH_4 peaks were seen from H_2CO covered W(100) in Fig. 4.

Two desorption spectra for CO_2 desorbed from H_2CO layers adsorbed on W(111) at $\sim$104 K are shown in Fig. 11. The H_2CO exposure necessary to produce measurable CO_2 evolution is $\sim 2 \times 10^{-5}$ Torr s. As in the case of W(100), the dominant features in the desorption spectra are the sharp peak at $\sim$130 K and a peak at $\sim$550 K. In addition, a small peak at $\sim$280 K is evident in Fig. 11. We cannot exclude the possibility that the sharp 130-K CO_2 peak originates from a small amount of impurity CO_2 present in our H_2CO which is physically adsorbed on our surfaces at higher exposures.

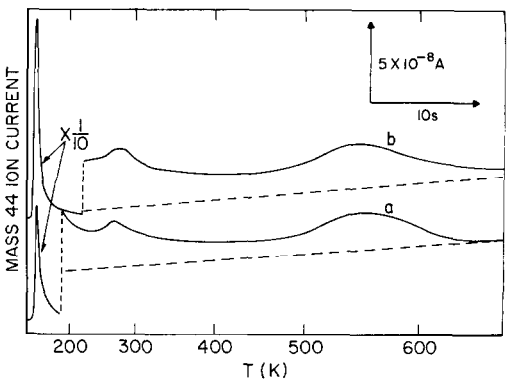

FIG. 11. Desorption spectra for CO_2 desorbed from an H_2CO layer adsorbed on W(111) at $T_0 \simeq$ 104 K. Mass 44 ion current is plotted vs crystal temperature (K).

Curve	H_2CO exposure ($\times 10^{-6}$ Torr s)
a	36
b	33

F. Comparison of Decomposition Product Yields on W(100) and W(111)

Figures 12–14 are semilogarithmic plots of the various desorption product yields as a function of H_2CO exposure on the two crystals. The most obvious difference between the yields from the two crystals is

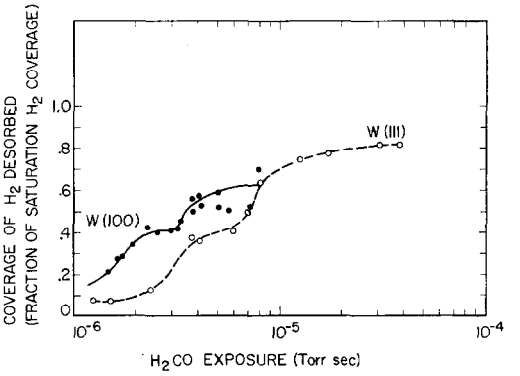

FIG. 12. Total yield of hydrogen desorbed following H_2CO adsorption on tungsten single crystals vs the H_2CO exposure (Torr s). Hydrogen desorption yield is expressed as the fraction of hydrogen desorbed relative to saturation coverage of pure H_2 on the appropriate crystal. Adsorption temperatures were $T_0 \simeq$ 104 K [W(111)]; $T_0 \simeq$ 110 K [W(100)].

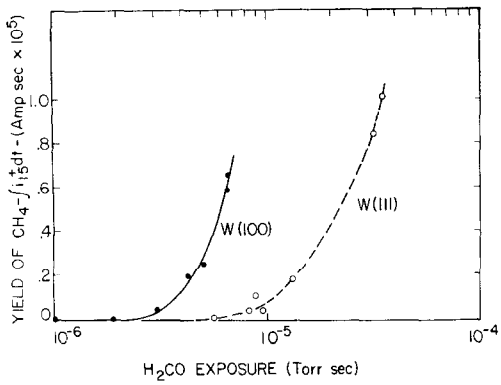

FIG. 13. Desorption yield of CH_4 following adsorption of H_2CO on W(100) and W(111) vs H_2CO exposure (Torr s). The desorption yield is expressed as the integral of flash desorption traces including those of Figs. 4 and 10 (A s). Adsorption temperatures were: $T_0 \simeq 104$ K [W(111)]; $T_0 \simeq 110$ K [W(100)].

the higher H_2CO exposure necessary to produce desorption of products from the W(111) crystal in comparison to the W(100). A possible cause for this difference is suggested as follows. Tamm and Schmidt (*10*) have found for pure hydrogen adsorption that the saturation coverage of H_2 on W(111) is 1.75 times greater than the saturation coverage on W(100). Thus, in the event of similar sticking probabilities

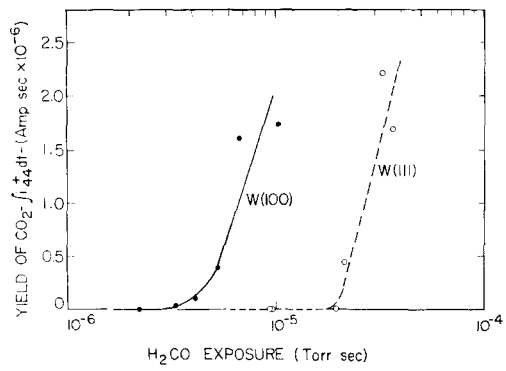

FIG. 14. Desorption yield of CO_2 following adsorption of H_2CO on W(100) and W(111) vs H_2CO exposure (Torr s). Desorption yield is expressed as the integral of flash desorption traces, including those of Figs. 5 and 11 (A s). Adsorption temperatures were: $T_0 \simeq 104$ K [W(111)]; $T_0 \simeq 110$ K [W(100)].

for H_2CO on the two planes, it is possible that a higher H_2CO exposure (and hence, a higher H_2CO coverage) is necessary to produce the critical coverages on W(111) which lead to the appearance of CH_4 and CO_2 in thermal desorption. A sticking probability of H_2CO on W(111) smaller than that for H_2CO on W(100) would produce a similar effect; however, accurate sticking probability measurements in this system using conventional gas uptake measurements were impossible due to wall effects involving H_2CO. Furthermore, slight changes made between experiments in the crystal support and cooling assembly, as well as small differences in the ion gauge behavior (*22*) may have affected the accuracy of the intercomparison of exposure scales.

G. Work Function Measurements During Adsorption of H_2CO at ~110 K and 300 K

An electron gun was used to measure the changes in the work function of the tungsten single crystal surfaces during adsorption of H_2CO. The work function change as a function of H_2CO exposure on the surfaces held at ~110 K is shown in Fig. 15. The results on both crystal surfaces are quite similar; the work function initially increases above the clean surface value. The onset of the rapid decrease in work function change corresponds roughly to the threshold exposures for the appearance of CH_4 in the desorption spectra (see Fig. 13). Similar work function measurements previously reported (*12*) have demonstrated that a work function decrease below the clean surface value is *not observed* for coadsorbed mixtures of H_2 + CO on W(100) at ~100 K. This further supports the view that the work function decrease seen at high H_2CO exposures is due either to undissociated H_2CO or to the formation of complex adsorbed intermediates.

The work function behavior during adsorption of H_2CO on W(100) and W(111) at 300 K is shown in Fig. 16. These results are qualitatively similar to the data of

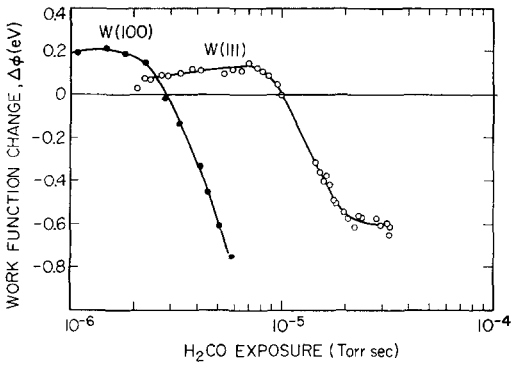

FIG. 15. Work function changes as a function of H_2CO exposure on W(100) and W(111) at ~110 K.

Fig. 15 and verify the stability of the adsorbed H_2CO and/or the complex intermediates even at 300 K. The limiting values of the work function changes are different at the two adsorption temperatures, presumably due in large part to the lower saturation coverages at the higher adsorption temperature.

H. Field Emission Observations of H_2CO Decomposition

A field emission microscope containing a single crystal tungsten emitter and a phosphor covered anode was attached as an appendage to the vacuum system used in these studies; it has been described previously (*16*). Our primary interest in using the field emission microscope was in a search for a residual oxygen or carbon layer following the adsorption and thermal decomposition of H_2CO. Two types of field emission experiments were performed. With the emitter initially held at 300 K with a background pressure of 2×10^{-8} Torr of H_2CO present, the emitter was flashed clean (2500 K), then cooled to adsorb H_2CO. Upon repeated heating to ~1650 K, no residual decomposition product was visible: the field emission pattern from the heated emitter appeared clean. H_2 and CO are readily desorbed below 1650 K, but carbides and oxides would be stable to 2000 K or above. The emitter was then cooled to ~77 K and dosed with H_2CO for an exposure of $\sim 1 \times 10^{-5}$ Torr s. After reducing the H_2CO background pressure, the emitter was rapidly heated to ~1650 K and a "crossbones" pattern indicative of adsorbed oxygen was seen (*23*); this pattern was stable until the emitter was heated well above 2000 K. The conclusions from these experiments are: (a) At low H_2CO exposures, the H_2CO decomposes and desorbs cleanly (as H_2 and CO) upon heating, leaving no oxygen or carbon residue; (b) At high H_2CO exposures, a small residual oxygen coverage remains on the surface after heating. Unfortunately, the persistent presence of a small amount of CO_2 as a gaseous contaminant following high H_2CO exposure cannot be definitely excluded as the source of the residual oxygen layer on the heated sample; it is known from field emission (*24*) and flash desorption (*15*) measurements with pure CO_2 on tungsten that dissociation to CO(ads) and O(ads) occurs.

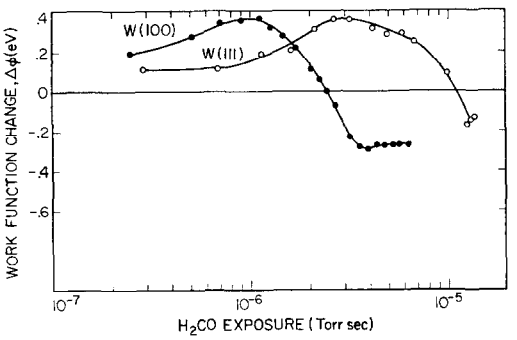

FIG. 16. Work function changes as a function of H_2CO exposure on W(100) and W(111) at 300 K.

IV. DISCUSSION

A. Thermochemistry of H_2CO Adsorption and Decomposition

As an aid to understanding the decomposition of adsorbed H_2CO on tungsten, it is of interest to consider the thermochemistry of H_2CO and its decomposition products (*25*). Consider the following gas phase reactions:

$$2H_2CO(g) \rightarrow CO_2(g) + CH_4(g), \quad (1)$$

$$H_2CO(g) \rightarrow H_2(g) + CO(g). \quad (2)$$

Reaction (1) is strongly exothermic with a reaction heat of $\Delta H^0(1) = -60.04$ kcal/

mole of products. Reaction (2) is only slightly exothermic with a reaction heat, $\Delta H^0(2) = -0.47$ kcal/mole. Both reactions exhibit a negative ΔG^0 at 298 K.

In order to assess the thermochemically different reaction paths on the surface, the heat of adsorption of the molecules must be known. Consider the alternate decomposition paths for adsorbed H_2CO:

$$2H_2CO(a) \rightarrow CO_2(a) + CH_4(a), \quad (3)$$

$$2H_2CO(a) \rightarrow 2H_2(a) + 2CO(a). \quad (4)$$

Gas phase thermochemical data (*25*), along with zero coverage heats of adsorption (or desorption) were used as follows:

$$-\Delta H_a(H_2) = 32 \text{ kcal/mole } (4, 5),$$

$$-\Delta H_a(CO) = 93 \text{ kcal/mole } (15),$$

$$-\Delta H_a(CH_4) = 7.5 \text{ kcal/mole } (11, 16),$$

$$-\Delta H_a(CO_2) = 109 \text{ kcal/mole } (26).$$

The first three values correspond to low coverage thermal desorption energies from W(100). The heat of adsorption for CO_2 on a W film is a calorimetric value; it appears that CO_2 in fact dissociates at low coverages to CO(a) + O(a) on W. Unfortunately, the heat of adsorption for H_2CO on W is not available. Using these values, the heats of reaction at low H_2CO coverages on W for reactions (3) and (4) are given by:

$$\Delta H(3) = -2\Delta H_a(H_2CO) + \Delta H^0(1) + \Delta H_a(CH_4) + \Delta H_a(CO_2)$$

$$= -2\Delta H_a(H_2CO) - 177 \text{ kcal.}$$

$$\Delta H(4) = -2\Delta H_a(H_2CO) + 2[\Delta H^0(2) + \Delta H_a(H_2) + \Delta H_a(CO)]$$

$$= -2\Delta H_a(H_2CO) - 251 \text{ kcal.}$$

If the heat of adsorption of H_2CO is less than 89 kcal/mole, then at low coverages both processes are exothermic; the exothermicity of reaction (4) is greater than that of reaction (3) by 74 kcal. It appears from our experimental thermal desorption data that on both W(100) and W(111) *at low H_2CO* coverages reaction (4) is favored on kinetic grounds.

As the coverage of adsorbed species is increased, the heat of adsorption of the various species will decrease. Consideration of the possible variations in ΔH_a for the various species (*4, 5, 11, 12, 15*) indicates that the exothermicity *difference* between reactions (3) and (4) will probably decrease, but both processes will remain exothermic and probably thermodynamically possible. Thus, *thermodynamic* exclusion of reaction (4) at higher coverages is not likely; instead we must postulate that as coverage increases, steric crowding factors induce the formation of new kinds of adsorbed intermediates other than H(ads) and CO(ads) and these intermediates liberate both CH_4(g) and CO_2(g) upon heating.

B. Kinetics of H_2CO Decomposition on Tungsten

At *low* H_2CO exposures and coverages, the following experimental evidence supports a model of low temperature dissociative adsorption of H_2CO on tungsten to yield H(ads) + CO(ads):

1. H_2 and CO are the only desorption products; mixtures of H(ads) and CO(ads) also yield only H_2 and CO upon desorption (*12*).
2. H_2 desorption states resemble (in their desorption temperature range) the hydrogen states produced by coadsorption of CO and H_2 on W(100) (*12*).
3. The work function rises during early stages of H_2CO adsorption; this is also seen for mixtures of H(ads) and CO(ads) on W(100) (*12*).

At higher H_2CO exposures however, a number of new experimental features are observed which indicate that at higher coverages a new kind of adsorption complex is produced, i.e., HCO(ads), H_2CO(ads) or more complex associated species. Surface complex formation at higher coverages is indicated by the following observations:

1. CH_4 and CO_2 are new products of desorption, never seen from mixtures of H(ads) and CO(ads) (*12*).
2. CH_4 desorbs from the H_2CO layer at temperatures several hundred degrees higher than the desorption temperature for pure CH_4 adsorbed alone on tungsten (*11, 16*). The rate controlling step in CH_4 de-

sorption is apparently the decomposition of surface complexes.

3. H_2 desorption behavior departs from that observed with H(ads) and CO(ads) mixtures. A new desorption peak above 400 K is observed at higher H_2CO exposures on W(100), and is not seen for mixtures of H(ads) and CO(ads).

4. The work function passes through a maximum and at higher H_2CO exposure falls sharply; this is not seen for mixtures of H(ads) and CO(ads) on W(100) (*12*).

5. The H_2 coverage from H_2CO increases monotonically on W(111) as exposure is increased; in contrast, H(ads) can be displaced by CO at 104 K on W(111).

6. At high H_2CO exposures on W(100) at 273 K, significant quantities of H_2 are observed upon flash desorption; in contrast, H(ads) can be completely displaced by CO at 273 K on W(100) (*12*).

C. Kinetics of Desorption of H_2CO Decomposition Products

All of the desorption spectra corresponding to desorption of H_2 and CH_4 from high exposures of H_2CO on W(100) and W(111) have one feature in common: the distinct desorption peaks observed are too broad to be explained by simple first or second order desorption mechanisms with "normal" preexponential terms and constant desorption energies. For a simple desorption process, the rate of desorption may be expressed as

$$-\frac{d\sigma}{dt} = \sigma^n \nu_n e^{-E_d/RT} \qquad (5)$$

where σ is the coverage of the species in question (atoms or molecules/cm^2), ν is the preexponential term, E_d is the desorption activation energy, R is the gas constant, T is temperature (K), and n is the desorption order ($n = 1$ for first order desorption; $n = 2$ for second order desorption). The functional form of desorption spectra for first or second order desorption processes during a linear increase of temperature with time has been discussed previously (*27*, *16*). A good example of a nearly ideal first order desorption spectrum is provided by the β_1 state of hydrogen desorbing from W(100) [see Fig. 2a and Refs. (*4*, *5*)]. The β_1 peak is quite sharp, having a full width at half maximum of ($\Delta T_{1/2}$) $\simeq$ 40 K.

In order to compare the present experimental data with model calculations of desorption spectra, we will examine the desorption of CH_4 from H_2CO adsorbed on W(100) (see Fig. 4). Physically adsorbed CH_4 on W(100) desorbs with first order kinetics [see broken curve, Fig. 4 and Ref. (*16*)] and we assume, for the sake of the calculations, that CH_4 desorbs from an H_2CO layer following first order kinetics. Model calculations of simple first order desorption spectra having peaks located at 280 and 505 K yield the results shown in Table 1. Assuming knowledge of both the peak temperature and ν yields values of E_d and $\Delta T_{1/2}$. It is clear that the $\Delta T_{1/2}$ values for the experimental peaks illustrated in Table 1 are much too large to be explained by first order desorption with a normal (10^{13} s^{-1}) preexponential term. Similar conclusions may be drawn regarding the desorption of the other decomposition products of H_2CO.

A variety of reasons may be advanced to explain the large $\Delta T_{1/2}$ values. Large entropy decreases accompanying the formation of the desorbing molecule would cause a drastic decrease in ν and a corresponding increase in $\Delta T_{1/2}$. Complex surface kinetic processes might also be expected to affect

TABLE 1
MODEL CALCULATION OF KINETIC PARAMETERS FOR FIRST ORDER DESORPTION

First order desorption peak position T_m (K)	Experimental[a] $\Delta T_{1/2}$ (K)	Model calculations E_d (kcal/mole)	ν(s^{-1})	$\Delta T_{1/2}$(K)
280	150	16.2	1×10^{13}	26
		9.9	1×10^{8}	36
		4.2	1×10^{3}	72
505	130	29.9	1×10^{13}	42
		18.9	1×10^{8}	64
		8.5	1×10^{3}	127

[a] Data taken from desorption spectra of Fig. 4 corresponding to desorption of CH_4 from adsorbed H_2CO.

the apparent desorption kinetics, particularly if the rate-controlling step for desorption is really decomposition and/or diffusion. These latter effects are to be expected in view of the complexity of the H_2CO desorption products. Overlapping, unresolved substates or coverage-dependent activation energies as well as higher order desorption kinetics would cause broadened desorption peaks. Attempts to characterize the desorption of the H_2CO decomposition products by idealized single-process rate laws are simply not appropriate.

D. The Nature of the Surface Complex Produced by H_2CO Adsorption on Tungsten

The following properties of the surface complex have been observed:

1. The complex possesses a positive dipole oriented outward from the surface, leading to a work function decrease.
2. The complex yields methane in two desorption stages at about 300 and 500 K during programmed heating.
3. The complex yields H_2 in two desorption stages at about 300 and 500 K during programmed heating.
4. The complex yields CO_2 in a high temperature desorption stage above $\sim$500 K.

We cannot be specific about the structure of the surface complex formed at higher coverages in the presence of H(ads) previously generated by fragmentation of H_2CO at lower coverages. Structures such as

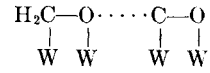

(6)

or

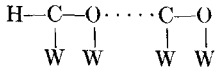

(7)

could be subject to attack by H(ads) to yield CO_2(ads) plus either CH_2(ads) or CH_3(ads). Further attack during heating could then lead to CH_4(g) and CO_2(g) evolution. Since the maximum H_2 evolution and CH_4 evolution rates seem to occur together in two stages, it may be that H(ads) availability or mobility may be rate determining in the production of both CH_4(g) and H_2(g). The surface-catalyzed combination of species such as CH_3(ads) could then lead to the small yields of C_2H_6 or higher hydrocarbons.

The field emission evidence showing that a carbon residue does not remain on tungsten following H_2CO decomposition suggests that very reactive carbon-containing species are involved; the reactivity of these species with H(ads) is postulated to result in desorption of CH_4 before carbide formation becomes possible at elevated temper-

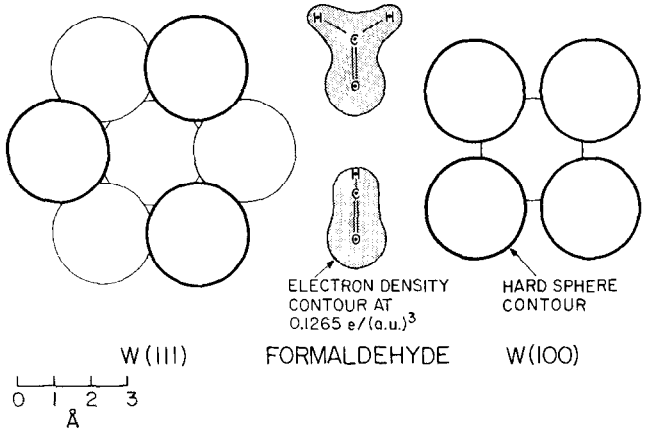

FIG. 17. Models of structure of tungsten crystal planes and two views of the H_2CO molecule (*28*). The topmost plane of tungsten atoms is indicated by the dark circle.

TABLE 2
COMPARISON OF H_2CO ADSORPTION BEHAVIOR ON W(100) AND W(111)

Experimental feature	W(100)	W(111)
Products of desorption at low H_2CO coverage	$H_2 + CO$	Same
New products of desorption at high H_2CO coverages	$CH_4 + CO_2$	Same
Number of H_2 desorption stages above 200 K at highest H_2CO coverage	Two	Two
Maximum number of stages of H_2 desorption above 200 K at intermediate H_2CO coverages	Three	Three
Comparison of H_2 desorption spectra from medium coverages of H_2CO with spectra from mixtures of H_2 and CO	Good qualitative correlation	Poor qualitative correlation
Number of CH_4 desorption stages above 200 K at highest H_2CO coverage	Two	Two
Number of CO_2 desorption stages at highest H_2CO coverage	Three	Three
Contribution of lowest temperature CO_2 state compared to other states	Small	Approximately equal
Double plateau in H_2 yield vs exposure	Yes	Yes
Work function behavior at low H_2CO exposures	$\Delta\phi > 0$ $\Delta\phi_{max} = +0.2$ V	$\Delta\phi > 0$ $\Delta\phi_{max} = +0.13$ V
Work function behavior at high H_2CO exposures	$\Delta\phi < 0$	$\Delta\phi < 0$

atures, as studied in a previous investigation (*16*).

E. Comparison of the Chemistry of Formaldehyde Decomposition on the Two Crystal Planes of Tungsten

In Fig. 17 is shown the structure of the two W crystal planes studied in this work, along with a representation of the shape and size of the free H_2CO molecule (*28*). Because of the approximate trigonal symmetry about the C atom in H_2CO, it was expected that the threefold symmetric W(111) plane would exhibit different activity and perhaps produce different products with H_2CO when compared to W(100). In fact, as shown in Table 2, there are a large number of qualitative similarities observed for the two planes, indicating that in this case surface crystallography plays a secondary role in determining the chemical and electronic behavior of H_2CO during adsorption. Our experiments are probably observing the intrinsic properties of surface complexes which are similar on both planes. In contrast to this, the desorption behavior of pure hydrogen layers is very characteristic of the tungsten plane involved as can be seen by comparing Figs. 2a and 8a.

ACKNOWLEDGMENT

We gratefully acknowledge a valuable discussion with Dr. Joel Liebman, NRC-NBS Postdoctoral Research Associate.

REFERENCES

1. REDHEAD, P. A., *Trans. Faraday Soc.* **57**, 641 (1961).
2. EHRLICH, G., *in* "Advances in Catalysis" (D. D. Eley, H. Pines and P. B. Weisz, Eds.), Vol. 14, p. 255. Academic Press, New York, 1963.
3. YATES, J. T., JR., AND MADEY, T. E., *J. Chem. Phys.* **51**, 334 (1969).
4. TAMM, P. W., AND SCHMIDT, L. D., *J. Chem. Phys.* **51**, 5352 (1969); **52**, 1150 (1970).
5. MADEY, T. E., AND YATES, J. T., JR., "Structure et Proprietes des Surfaces des Solides," No. 187, p. 155. CNRS Paris, 1970.
6. CLAVENNA, L. R., AND SCHMIDT, L. D., *Surface Sci.* **22**, 365 (1970).
7. BARFORD, B. D., AND RYE, R. R., *J. Vac. Sci. Technol.* **9**, 673 (1972).
8. MAY, J. W., SZOSTAK, R. J., AND GERMER, L. H., *Surface Sci.* **15**, 37 (1969).
9. GASSER, R. P. H., AND MARSAY, C. J., *Surface Sci.* **20**, 116 (1970).
10. TAMM, P. W., AND SCHMIDT, L. D., *J. Chem. Phys.* **54**, 4775 (1971).
11. MADEY, T. E., *Surface Sci.* **29**, 571 (1972).
12. YATES, J. T., JR., AND MADEY, T. E., *J. Chem. Phys.* **54**, 4969 (1971).

13. ANDERSON, J., AND ESTRUP, P. J., *J. Chem. Phys.* **46,** 563 (1967).

14. YATES, J. T., JR., AND KING, D. A., *Surface Sci.* **32,** 479 (1972).

15. CLAVENNA, L. R., AND SCHMIDT, L. D., *Surface Sci.* **33,** 11 (1972).

16. YATES, J. T., JR., AND MADEY, T. E., *Surface Sci.* **28,** 437 (1971).

17. MARSHALL, M. J., AND STEDMAN, D. F., *Trans. Roy. Soc. Can. Sect. 3* **17,** 53 (1923).

18. BALDWIN, V. H., JR., AND HUDSON, J. B., *J. Vac. Sci. Technol.* **8,** 49 (1971).

19. CALVERT, J. G., AND STEACIE, E. W. R., *J. Chem. Phys.* **19,** 176 (1951).

20. Amer. Petrol. Inst. Res. Proj. 44, "Mass Spectral Data," 1959.

21. WALKER, J. F., "Formaldehyde" (Amer. Chem. Soc. Monogr. Ser.), 3rd ed., pp. 37–38. Reinhold, New York, 1964.

22. YOUNG, J. R., *J. Vac. Sci. Technol.* **10,** 212 (1973).

23. Typical field emission patterns for oxygen on tungsten have been reported by a number of investigators. See, for example, R. Gomer and J. K. Hulm, *J. Chem. Phys.* **27,** 1364 (1957).

24. HAYWARD, D. O., AND GOMER, R., *J. Chem. Phys.* **30,** 1617 (1959).

25. COX, J. D., AND PILCHER, G., "Thermochemistry of Organic and Organometallic Compounds," Academic Press, London, 1971.

26. HAYWARD, D. O., AND TRAPNELL, B. M. W., "Chemisorption," p. 205. Butterworths, Washington, 1964.

27. REDHEAD, P. A., *Vacuum* **12,** 203 (1962).

28. DUNNING, T. H., JR., AND WINTER, N. W., *J. Chem. Phys.* **55,** 3360 (1971).